

Single Particle Spectroscopies of p -wave and d -wave Interacting Bose Gases in Normal Phase

Zeqing Wang and Ran Qi*
*Department of Physics, Renmin University of China,
 Beijing, 100872, P. R. China*

(Dated: December 5, 2023)

Motivated by experiments of interacting quantum gases across high partial wave resonance, we investigated the thermodynamic properties as well as single particle spectrums of Bose gases in normal phase for different interaction strengths both for p -wave and d -wave interactions. The free energy, contact density, momentum distributions, and self-energies of single particle Green's functions are obtained in the spirit of ladder diagram approximations. Radio frequency (RF) spectrum, as an important experimental approach to detect Feshbach molecules or interaction effect, is calculated at different temperatures. A reversed temperature dependence on the BEC side and BCS side is identified for both p -wave and d -wave interactions. An estimation for the signal of RF spectra under typical experimental conditions is also provided.

I. INTRODUCTION

Ultracold atomic gases, due to their tunable interaction strength by Feshbach resonance (FR), provide an ideal platform to realize different kinds of quantum phases [1–3]. In contrast to the widely studied s -wave FRs, the high partial wave FRs with nonzero relative angular momentum support various kinds of topological quantum matters such as topological superfluids and majorana zero modes. In recent years, interacting quantum gases across p -wave and d -wave resonance have been realized and used to investigate the few-body and many-body problems in many experiments [4–15]. Some g -wave Feshbach resonances have also been studied in recent experiments [13, 16].

Spectroscopy is a powerful tool to investigate the rich many-body physics in ultracold quantum gases. Various spectroscopies are used in ultracold quantum gas experiments, for example, RF spectroscopy, Bragg spectroscopy, and lattice modulation spectroscopy [17]. The RF spectral response of unitary ^6Li Fermi gas at different temperatures is observed in [18]. RF response of impurities interacting with a quantum gas at finite temperature is investigated theoretically in [19, 20]. However, RF spectroscopy of high partial wave interacting quantum gases is rarely studied.

Motivated by the recent experiments for high partial wave interacting quantum gases, we investigated the RF spectroscopy and momentum distribution of quantum Bose gases across p -wave and d -wave resonance in different interaction strength regions. The low energy scattering amplitude can be characterized by the scattering volume v_m (super-volume D_m) for p -wave (d -wave) interaction whose definition will be given in Sec. II. In experiments, v_m (D_m) can be tuned from negative to positive infinity by tuning the magnetic field [4, 14, 15],

as illustrated schematically in Fig. 1. When $v_m > 0$ ($D_m > 0$), there exists a shallow bound state with infinite lifetime, while for $v_m < 0$ ($D_m < 0$), there is a quasi-bound state with positive binding energy due to the centrifugal barrier. As shown in Fig. 1, this quasi-bound state has a finite lifetime τ proportional to $1/E_b^{3/2}$ for p -wave ($1/E_b^{5/2}$ for d -wave) with E_b being the binding energy. The inverse lifetime $1/\tau$ characterizes the coupling strength between the quasi-bound state and the scattering states which have important influences in the RF spectrum. In analogy to the BEC-BCS crossover of Fermions, we will call the $E_b < 0$ region BEC side and the $E_b > 0$ region BCS side for convenience in this article.

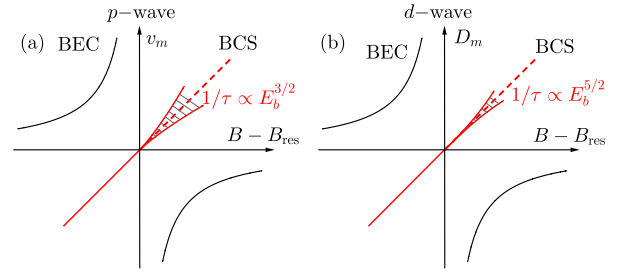


FIG. 1. Schematic of different interaction regions. The black solid lines show the scattering volume v_m (super-volume D_m) as a function of magnetic field B , and diverges at resonance magnetic field B_{res} . The red solid lines indicate the shallow bound state on the BEC side. On the BCS side, the red dashed lines indicate the quasi-bound state with positive binding energy and finite lifetime τ represented by the shaded area.

We first introduce our two-channel model in Sec. II. The self-energy of single particle Green's function is obtained within ladder diagram approximation or the so-called Nozières and Schmitt-Rink (NSR) scheme [21, 22]. In Sec. III, the contact density is also derived within NSR scheme through the adiabatic theorem [23, 24, 29], and is compared with the results from high temperature virial

* qiran@ruc.edu.cn

expansion. Next, in Sec. IV, we present the results of single particle spectral function in which a clear anisotropic dependence in the momentum will be shown. The momentum distributions, obtained by integrating the single particle spectral function over frequency, are analyzed in Sec. V. Finally, results of RF spectrum are presented and an estimation of signal strength (in terms of the atom transfer rate to final state) under typical experimental parameters is provided in Sec. VI.

II. MODEL

A. Hamiltonian

For strongly interacting Bose atoms across a p -wave or d -wave FR, the Hamiltonian can be written as the following two-channel model [22],

$$\begin{aligned} \hat{H}_0 = & \sum_{\mathbf{k}, \sigma=\sigma_{1,2}} \xi_{\mathbf{k}} \hat{a}_{\mathbf{k},\sigma}^\dagger \hat{a}_{\mathbf{k},\sigma} + \sum_{\mathbf{q}, m} (\xi_{\mathbf{q},b} - \nu_m) \hat{b}_{\mathbf{q},m}^\dagger \hat{b}_{\mathbf{q},m} \quad (1) \\ & + \sqrt{\frac{4\pi}{V}} \sum_{\mathbf{k}, \mathbf{q}, m} \left[g_m k^l Y_{l,m}(\hat{\mathbf{k}}') \hat{b}_{\mathbf{q},m}^\dagger \hat{a}_{-\mathbf{k}+\mathbf{q},\sigma_1} \hat{a}_{\mathbf{k},\sigma_2} + \text{h.c.} \right], \end{aligned}$$

where $\hat{a}_{\mathbf{k},\sigma}$ and $\hat{b}_{\mathbf{q},m}$ are annihilation operators for atoms and closed channel dimers and σ labels the different hyperfine states. The first and second terms correspond to the energy of free atoms and dimers. $\xi_{\mathbf{k}} = \frac{\hbar^2 k^2}{2M} - \mu$ is the kinetic energy of an atom measured from its chemical potential μ . $\xi_{\mathbf{q},b} = \frac{\hbar^2 q^2}{4M} - 2\mu$ is the kinetic energy for a dimer measured from its chemical potential 2μ . To simplify the notations, we will set $M = k_B = \hbar = 1$ (k_B being the Boltzmann constant) throughout the rest part of this paper. ν_m is the detuning for m channel with m standing for magnetic quantum number. The last term in the Hamiltonian describes the coupling between the atom channel and the dimer channel with $l = 1, 2$ corresponding to p - and d -wave resonances respectively [4, 14, 15]. $m = 0, \pm 1, \dots, \pm l$ represent the quantum number of \hat{l}_z . $\mathbf{k}' = \mathbf{k} - \mathbf{q}/2$ is the relative momentum of two incoming atoms that form the dimer, and $k' = |\mathbf{k}'|$, $\hat{\mathbf{k}}' = \mathbf{k}'/k'$. V is the volume of the system. g_m is the strength of coupling and $Y_{l,m}(\theta, \phi)$ are the spherical harmonic functions.

Because the Bosonic wave function must be symmetric under the exchange of two identical Bosons, p -wave interaction can only exist between two different hyperfine states. As a result, for p -wave interaction we consider a two components Bose gas where the summation of σ is over $\sigma_{1,2} = 1, 2$, while for d -wave interaction we consider a single component Bose gas with $\sigma_1 = \sigma_2$ and the summation over σ drops out. In analogy to the Fermi gas, we will define a characteristic momentum unit k_F as $k_F^3 = 3(6)\pi^2 n_{\text{total}}$ for the two(single) component Bose gas, and a corresponding energy unit $E_F = k_F^2/2$. Here n_{total} is the total particle number density of Bose gas.

The bare parameters ν_m and g_m are related to the low energy scattering parameters through a set of renormal-

ization relations [22, 24, 25]. For p -wave interaction, we have

$$\frac{\nu_m}{g_m^2} = \frac{1}{4\pi} v_{p,m}^{-1} - \frac{1}{V} \sum_{\mathbf{k}} 1, \quad (2)$$

$$\frac{1}{g_m^2} = \frac{1}{4\pi} R_{p,m}^{-1} - \frac{1}{V} \sum_{\mathbf{k}} \frac{1}{k^2}, \quad (3)$$

while for d -wave, we have

$$\frac{\nu_m}{g_m^2} = \frac{1}{4\pi} D_m^{-1} - \frac{1}{V} \sum_{\mathbf{k}} k^2, \quad (4)$$

$$\frac{1}{g_m^2} = \frac{1}{4\pi} v_{d,m}^{-1} - \frac{1}{V} \sum_{\mathbf{k}} 1, \quad (5)$$

$$R_{d,m}^{-1} = \frac{4\pi}{V} \sum_{\mathbf{k}} \frac{1}{k^2}, \quad (6)$$

where the meaning of physical parameters D_m , $v_{p(d),m}$ and $R_{p(d),m}$ will be clear in the two-particle vertex function presented in the next section.

B. Self-energy

The self-energy of single particle Green's function is obtained within the ladder diagram approximation as shown in Fig. 2 [21, 22]:

$$\Sigma(\mathbf{k}, i\Omega_\nu) = -\frac{1}{\beta} \sum_{\mathbf{q}} \sum_{\omega_n} \Gamma(\mathbf{q}, \mathbf{k}', i\omega_n) G_0(-\mathbf{k} + \mathbf{q}, i\omega_n - i\Omega_\nu), \quad (7)$$

where $\Omega_\nu = 2\nu\pi/\beta$ and $\omega_n = 2n\pi/\beta$ are Bose mat-

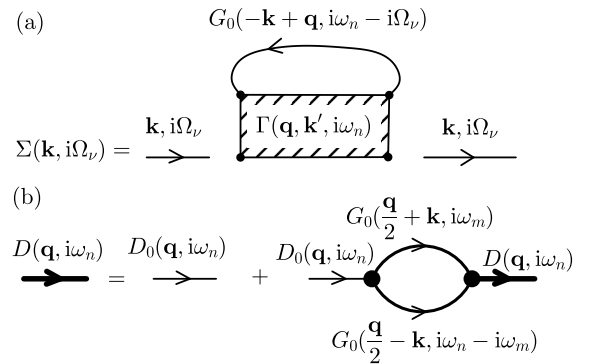


FIG. 2. Feynman diagram for (a) the self-energy of atoms and (b) the Green's function of dimers.

subara frequencies with $\beta = 1/T$ is the reciprocal of temperature. $G_0(-\mathbf{k} + \mathbf{q}, i\omega_n - i\Omega_\nu) = 1/(i\omega_n - i\Omega_\nu - \xi_{-\mathbf{k}+\mathbf{q}})$ is Matsubara Green's function for free atoms and $\Gamma(\mathbf{q}, \mathbf{k}', i\omega_n)$ is the two-particle vertex function within

ladder approximation [26],

$$\Gamma(\mathbf{q}, \mathbf{k}', i\omega_n) = \sum_m \frac{4\pi}{V} g_m^2 k'^{2l} \left| Y_{l,m}(\hat{\mathbf{k}}') \right|^2 D(\mathbf{q}, i\omega_n), \quad (8)$$

which describes the scattering between two atoms with the center of mass momentum \mathbf{q} and relative momentum \mathbf{k}' . $D(\mathbf{q}, i\omega_n)$ is the Matsubara Green's function of dimers formed by two atoms, which can be calculated by the Dyson equation in Fig. 2(b):

$$D(\mathbf{q}, i\omega_n) = \frac{1}{\frac{1}{D_0(\mathbf{q}, i\omega_n)} + g_m^2 \chi_{pp}(\mathbf{q}, i\omega_n)}, \quad (9)$$

where $D_0(\mathbf{q}, i\omega_n) = 1/(i\omega_n - \xi_{\mathbf{q},b} + \nu_m)$ is the free dimer propagator. χ_{pp} is the particle-particle bubble

$$\begin{aligned} \chi_{pp}(\mathbf{q}, i\omega_n) &= \frac{4\pi}{V} \sum_{\mathbf{k}} k^{2l} |Y_{l,m}(\hat{\mathbf{k}})|^2 \\ &\times \frac{1}{\beta} \sum_{\omega_m} G_0\left(\frac{\mathbf{q}}{2} + \mathbf{k}, i\omega_m\right) G_0\left(\frac{\mathbf{q}}{2} - \mathbf{k}, i\omega_n - i\omega_m\right). \end{aligned} \quad (10)$$

The divergent summation over \mathbf{k} can be renormalized by the renormalization relations in Sec. II A. Therefore we can write the two-particle vertex function in a renormalized form for each m channel:

$$\Gamma_m^p(\mathbf{q}, \mathbf{k}', i\omega_n) = \frac{4\pi \frac{4\pi}{V} k'^2 |Y_{1,m}(\hat{\mathbf{k}}')|^2}{\frac{1}{v_{p,m}} + \frac{Z}{R_{p,m}} + 4\pi R_{pp}^p}, \quad (11)$$

$$\Gamma_m^d(\mathbf{q}, \mathbf{k}', i\omega_n) = \frac{4\pi \frac{4\pi}{V} k'^4 |Y_{2,m}(\hat{\mathbf{k}}')|^2}{\frac{1}{D_m} + \frac{Z}{v_{d,m}} + \frac{Z^2}{R_{d,m}} + 4\pi R_{pp}^d}, \quad (12)$$

where $Z = i\omega_n - \frac{q^2}{4} + 2\mu$ and the renormalized particle-particle bubble

$$R_{pp}^p = \chi_{pp} - \frac{1}{V} \sum_{\mathbf{k}} 1 - Z \frac{1}{V} \sum_{\mathbf{k}} \frac{1}{k^2}, \quad (13)$$

$$R_{pp}^d = \chi_{pp} - \frac{1}{V} \sum_{\mathbf{k}} k^2 - Z \frac{1}{V} \sum_{\mathbf{k}} 1 - Z^2 \frac{1}{V} \sum_{\mathbf{k}} \frac{1}{k^2}. \quad (14)$$

The superscripts p and d stand for p -wave case and d -wave case correspondingly.

A main difference for high partial wave interaction comparing to s -wave interaction is the existence of centrifugal barrier, which makes the coupling between the true or quasi-bound states and the many-body medium very weak. This allows us to neglect the contribution from the branch cut of the two-particle vertex function $\Gamma_m^{p,d}$ and only include their pole structure. Within this single pole approximation, the particle-particle propagator will take the following simple form

$$\Gamma_m^p(\mathbf{q}, \mathbf{k}', i\omega_n) = \frac{4\pi R_{p,m} \frac{4\pi}{V} k'^2 \left| Y_{1,m}(\hat{\mathbf{k}}') \right|^2}{i\omega_n - \xi_{\mathbf{q},b} - E_b^p}, \quad (15)$$

$$\Gamma_m^d(\mathbf{q}, \mathbf{k}', i\omega_n) = \frac{4\pi v_{d,m} \frac{4\pi}{V} k'^4 \left| Y_{2,m}(\hat{\mathbf{k}}') \right|^2}{i\omega_n - \xi_{\mathbf{q},b} - E_b^d}. \quad (16)$$

where the molecular binding energies are given as $E_b^p = -R_{pm}/v_{pm}$ for p -wave and $E_b^d = -v_{dm}/D_m$ for d -wave.

After the standard frequency summation, the self-energy of single-particle Green's function within ladder diagram approximation is given as

$$\begin{aligned} \Sigma_m^p(\mathbf{k}, i\Omega_\nu) &= \sum_{\mathbf{q}} \frac{4\pi}{V} 4\pi R_{p,m} k'^2 \left| Y_{1,m}(\hat{\mathbf{k}}') \right|^2 \\ &\cdot \frac{N_B(\xi_{-\mathbf{k}+\mathbf{q}}) - N_B(\xi_{\mathbf{q},b} + E_b^p)}{i\Omega_\nu + \xi_{-\mathbf{k}+\mathbf{q}} - \xi_{\mathbf{q},b} - E_b^p}, \end{aligned} \quad (17)$$

$$\begin{aligned} \Sigma_m^d(\mathbf{k}, i\Omega_\nu) &= \sum_{\mathbf{q}} \frac{4\pi}{V} 4\pi v_{d,m} k'^4 \left| Y_{2,m}(\hat{\mathbf{k}}') \right|^2 \\ &\cdot \frac{N_B(\xi_{-\mathbf{k}+\mathbf{q}}) - N_B(\xi_{\mathbf{q},b} + E_b^d)}{i\Omega_\nu + \xi_{-\mathbf{k}+\mathbf{q}} - \xi_{\mathbf{q},b} - E_b^d}, \end{aligned} \quad (18)$$

where $N_B(\xi) = 1/(e^{\beta\xi} - 1)$ is the Bose-Einstein distribution function.

In experiments, high partial wave resonances are usually split due to anisotropy dipole-dipole interaction. According to [15], $m = 0$ is most important in the quantum degenerate regime. Therefore, we will only take the $m = 0$ channel into account and omit the subscript m without ambiguity in the following calculations.

III. EQUATION OF STATE AND CONTACT

In this section, we first determine the equation of state for our system. The particle density at fixed temperature and chemical potential can be derived through the thermodynamic potential, which within the ladder approximation is given as

$$\Omega = \Omega_0 + \Omega_{\text{int}}, \quad (19)$$

where $\Omega_0 = \sum_{\sigma} 1/\beta \sum_{\mathbf{k}} \ln[1 - e^{-\beta\xi_{\mathbf{k}}}]$ is the contribution of free atoms. Ω_{int} is the contribution of pair fluctuations due to the interaction between atoms, which can be derived using the Matsubara Green's function of dimers [21, 22],

$$\Omega_{\text{int}} = \frac{1}{\pi} \sum_{\mathbf{q}} \int_{-\infty}^{\infty} d\omega \frac{1}{e^{\beta\omega} - 1} \delta(\mathbf{q}, \omega) \quad (20)$$

where the phase $\delta(\mathbf{q}, \omega)$ is defined as $\delta(\mathbf{q}, \omega) = \text{Arg}[1/D(\mathbf{q}, \omega)]$. Follow the single pole approximation of last Section, δ can be written as,

$$\delta(\mathbf{q}, \omega) = \pi \Theta(\xi_{\mathbf{q},b} + E_b - \omega), \quad (21)$$

where $\Theta(x)$ is the Heaviside step function which is one for positive x and zero for negative x .

The total density can be expressed as the derivative of thermodynamic potential,

$$n_{\text{total}} = -\frac{1}{V} \frac{\partial \Omega}{\partial \mu} = -\frac{1}{V} \left(\frac{\partial}{\partial \mu} \Omega_0 + \frac{\partial}{\partial \mu} \Omega_{\text{int}} \right) \quad (22)$$

$$= n_0 + n_{\text{int}}, \quad (23)$$

where n_0 is the contribution of free atoms thermodynamic potential Ω_0 . n_{int} is the contribution from the pair fluctuation,

$$n_{\text{int}} = -\frac{1}{V} \frac{\partial \Omega_{\text{int}}}{\partial \mu} = \frac{1}{\pi^2} \int_0^\infty dq \cdot \frac{q^2}{e^{\beta(\frac{q^2}{4} - 2\mu + E_b^p)} - 1}. \quad (24)$$

Besides the particle density, we can also get the contact from the thermodynamic potential, which is an important parameter for many body systems [27–29]. We can get the contact density for p -wave scattering volume v_p and d -wave super-volume D by adiabatic theorem [23, 24, 29]

$$C^p \equiv -\frac{1}{V} \frac{\partial}{\partial v_p^{-1}} \Omega^p \Big|_{T, \mu} \quad (25)$$

$$= \frac{R_p}{2\pi^2} \int_0^\infty dq \cdot q^2 N_B(\xi_{\mathbf{q},b} + E_b^p) = R_p \frac{n_{\text{int}}^p}{2}, \quad (26)$$

$$C^d \equiv -\frac{1}{V} \frac{\partial}{\partial D^{-1}} \Omega^d \Big|_{T, \mu} \quad (27)$$

$$= \frac{v_d}{2\pi^2} \int_0^\infty dq \cdot q^2 N_B(\xi_{\mathbf{q},b} + E_b^d) = v_d \frac{n_{\text{int}}^d}{2}. \quad (28)$$

The contact for different interaction strengths at different temperatures above the critical temperature are shown in Fig. 3 [22]. One can see that the d -wave contact is about three orders of magnitude smaller than that of p -wave contact (in units of E_F), which implies that the momentum distribution tails and the RF spectra tails for d -wave may also be much weaker than those of p -wave. We will see that this is indeed true as shown in Sec. V and VI.

Another interesting feature in Fig. 3 is that, the temperature dependence of contact density is smoothly reversed when the interaction strength changes from BEC side to BCS side. On the BEC side, the contact is mainly contributed from the dimmer state (true bound state) with negative binding energy, which tends to be broken when temperature becomes higher. As a result, the contact density becomes smaller when temperature increases. While on the BCS side, at higher temperature, more atoms are excited to positive energy that can be coupled to the quasi-bound state and thus contribute to a larger contact density. This reversed temperature dependence of contact is also manifested in RF spectra as will be shown in Fig. 8.

An alternative approach to calculate the contact density is the high temperature virial expansion, which becomes asymptotically exact in the limit $T \gg E_F$ [30, 31].

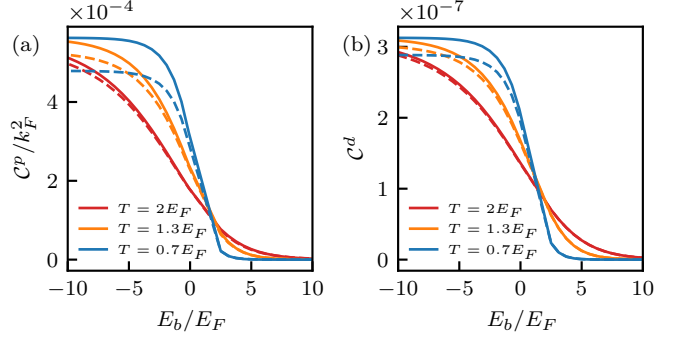


FIG. 3. The contact density as a function of binding energy at different temperatures for (a) p -wave and (b) d -wave. The solid lines are the results of Eq. (25) and Eq. (27). The dashed lines are the results of virial expansion. The scattering parameters are fixed at $k_F R_p = k_F v_d^{1/3} = 1/30$.

In virial expansion, the thermodynamic potential is expanded as a Taylor series of fugacity $z = e^{\beta\mu}$,

$$\Omega = -\frac{1}{\beta} Q_1 [z + b_2 z^2 + \mathcal{O}(z^3)], \quad (29)$$

where $Q_1 = 2V/\lambda_{\text{dB}}^3$ and $\lambda_{\text{dB}} = \sqrt{2\pi\beta}$ is the thermal de Broglie wavelength. The second virial coefficient b_2 can write as $b_2 = b_2^{(1)} + \Delta b_2$, where $b_2^{(1)}$ is the contribution of free atom thermodynamic potential Ω_0 . For Δb_2 , we use the Beth-Uhlenbeck formalism second virial coefficient, which is expressed in terms of phase shifts of a two-body scattering problem [30–32]

$$\frac{\Delta b_2}{\sqrt{2}} = \sum_i e^{-E_b^i/T} + \sum_l \frac{(2l+1)}{\pi} \int_0^\infty dk \frac{d\delta_l}{dk} e^{-\frac{\lambda_{\text{dB}}^2 k^2}{2\pi}}, \quad (30)$$

where the first summation is over all the two-body bound states, which only exist on the BEC side in our system. The phase shift in the second term is given by $k^3 \cot \delta_p = -1/v_p - k^2/R_p$ and $k^5 \cot \delta_d = -1/D - k^2/v_d - k^4/R_d$ [23, 24]. As shown in Fig. 3, the result from ladder approximation agrees well with that from virial expansion at higher temperature which provides a non-trivial check for our method.

IV. SINGLE PARTICLE SPECTRAL FUNCTION

In this section, we calculate the single particle spectral function, from which both the momentum distributions and RF spectrum will be derived in the following sections. For the convenience of numerical calculation of the single particle spectral function and many other properties of our system, we change the Matsubara Green's functions Eqs. (17) and (18) to retarded Green's functions by analytic continuation,

$$\Sigma(\mathbf{k}, i\Omega_\nu) \rightarrow \Sigma(\mathbf{k}, \Omega + i0^+). \quad (31)$$

The single particle spectral function is then written as [33],

$$A(\mathbf{k}, \Omega) = \frac{-2\text{Im}\Sigma(\mathbf{k}, \Omega)}{[\Omega - \xi_{\mathbf{k}} - \text{Re}\Sigma(\mathbf{k}, \Omega)]^2 + [\text{Im}\Sigma(\mathbf{k}, \Omega)]^2}. \quad (32)$$

In practice, we find that the term $\text{Re}\Sigma(\mathbf{k}, \Omega)$ is much smaller than the kinetic energy term $\xi_{\mathbf{k}}$ and thus can be safely neglected in Eq. (32) for both p - and d -wave resonance. The results are shown in Figs. 4 and 5.

The single particle spectral function of our system mainly contains the following two features: (i) the single particle excitation peak A_0 centered at the free atom excitation energy $\Omega = \xi_{\mathbf{k}}$ whose lifetime is determined by $\text{Im}\Sigma(\mathbf{k}, \Omega = \xi_{\mathbf{k}})$, and (ii) a threshold behavior from breaking a dimer denoted by A_{int} .

On the BEC side, A_0 is a delta peak with infinite lifetime,

$$A_0(\mathbf{k}, \Omega) = 2\pi\delta(\Omega - \xi_{\mathbf{k}}), \quad (33)$$

indicated by red lines in Figs. 4(a), 4(b) and 5(a), 5(b). This delta peak results from the fact that the denominator of $\Sigma(\mathbf{k}, \Omega = \xi_{\mathbf{k}})$, $\xi_{\mathbf{k}} + \xi_{-\mathbf{k}+\mathbf{q}} - \xi_{\mathbf{q},b} - E_b = (\mathbf{k} - \mathbf{q}/2)^2 - E_b$, is always positive when $E_b < 0$, which implies $\text{Im}\Sigma(\mathbf{k}, \Omega = \xi_{\mathbf{k}}) = 0$. Since the energy of an atom in the dimer is far away from the energy of a free atom, the spectral peak of the free atom and that of an atom in a dimer are well separated. This result suggests that there is no coupling between the dimer state with negative binding energy and scattering continuum with positive energy at this level of approximation.

On the BCS side, there is only quasi-bound state with positive binding energy which has finite coupling with the scattering continuum. As a result, the peak from the single particle excitation now gets a finite lifetime and merges into the dimer excitation, as shown in Figs. 4(c), 4(d) and 5(c), 5(d).

We can also see from Fig. 4 and Fig. 5 that the strength of the single particle spectral functions is very different at different momentum directions (here, we show the $\theta_k = 0$ and $\theta_k = \pi/2$ direction), which reflect the anisotropic nature of an isolated $m = 0$ FR of high partial wave interaction.

V. MOMENTUM DISTRIBUTION

In this section, we calculate the momentum distribution of atoms which can be expressed through the single particle spectral function obtained in Sec. IV,

$$N(\mathbf{k}) = \int_{-\infty}^{+\infty} \frac{d\Omega}{2\pi} N_B(\Omega) A(\mathbf{k}, \Omega). \quad (34)$$

In the limit $k = |\mathbf{k}| \rightarrow \infty$, we obtain the following asymptotic behavior for the momentum distribution:

$$N^p(\mathbf{k}) \approx \frac{16\pi^2}{k^2} \mathcal{C}^p |Y_{1,0}(\theta_k)|^2, \quad (35)$$

$$N^d(\mathbf{k}) \approx 16\pi^2 \mathcal{C}^d |Y_{2,0}(\theta_k)|^2, \quad (36)$$

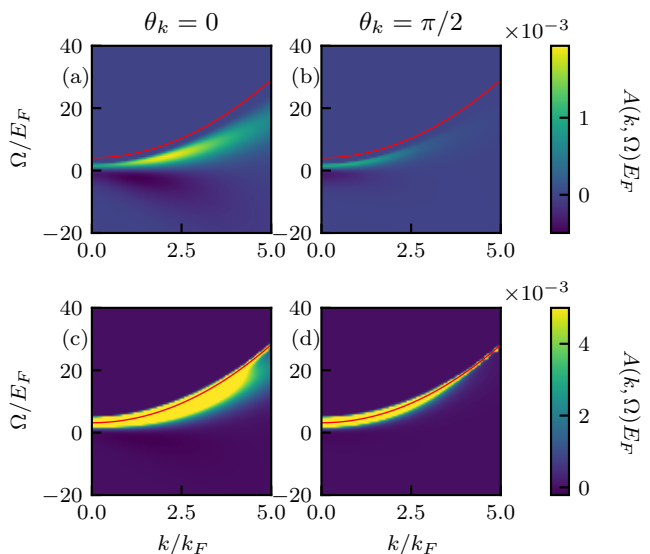


FIG. 4. Single particle spectral function for p -wave in different momentum direction. (a) and (b) are with binding energy $E_b = -2E_F$. (c) and (d) are with binding energy $E_b = 2E_F$. The red line in (a) and (b) indicates the free atom contribution. The red line in (c) and (d) indicates the location of $\Omega = \xi_{\mathbf{k}}$. The results are calculated at temperature $T = 2E_F$. Effective range is $k_F R_p = 1/30$. In order to see the peak clearly, we set the color bar limit 5×10^{-3} in (c) and (d).

where \mathcal{C}^p and \mathcal{C}^d is given by Eqs. (26) and (28). The above results verify the well known k^{-2} and k^0 tail as well as their relation with contacts for p -wave and d -wave interaction proposed in [23, 24].

The anisotropic nature of our system also manifests itself in the momentum distribution. Here we project the momentum distributions to Legendre function P_ν ,

$$N_\nu(k) = \int_0^\pi d\theta_k \cdot \sin \theta_k N(\mathbf{k}) P_\nu(\cos \theta_k). \quad (37)$$

The odd ν components are always zero which results from the spacial inversion symmetry. The even components are shown in Fig. 6. The analytic momentum tail in Eqs. (35) and (36) are indicated by the gray dashed lines, which agree well with the numerical results from Eq. (34).

VI. RF SPECTROSCOPY

Experimentally, the RF spectroscopy is measured by coupling the hyperfine state σ_2 to another hyperfine state labeled as σ_3 by RF pulse. This coupling can be described by the following Hamiltonian

$$\hat{H}_L = \sum_{\mathbf{k}} \left[\hat{a}_{\mathbf{k},\sigma_2}^\dagger \hat{a}_{\mathbf{k},\sigma_3} e^{i\omega' t} + \text{h.c.} \right], \quad (38)$$

where $\omega' = \nu_{\text{rf}} + \mu - \mu_3$ with ν_{rf} is the RF detuning. Then the RF spectrum, which describes the atoms transferring

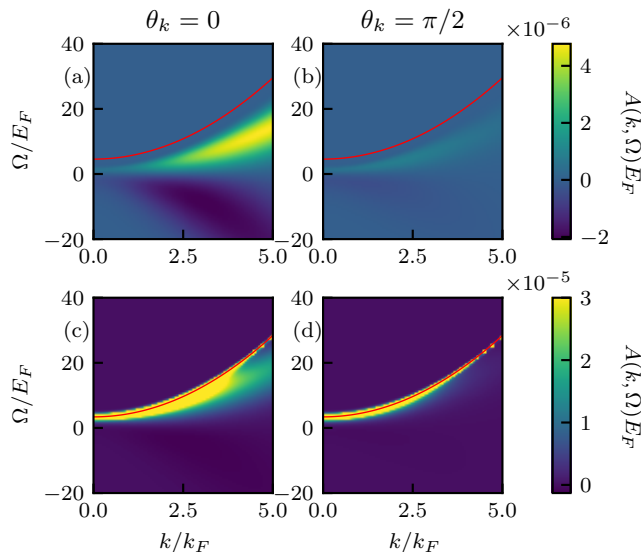


FIG. 5. Single particle spectral function for d -wave in different momentum direction. (a) and (b) are with binding energy $E_b = -2E_F$. (c) and (d) are with binding energy $E_b = 2E_F$. The red line in (a) and (b) indicates the free atom contribution. The red line in (c) and (d) indicates the location of $\Omega = \xi_{\mathbf{k}}$. The results are calculated at temperature $T = 2E_F$. Effective range is $k_F v_d^{1/3} = 1/30$. In order to see the peak clearly, we set the color bar limit 3×10^{-5} in (c) and (d).

rate from σ_2 to σ_3 state, can be expressed as a function of single particle spectral function [17],

$$I(\nu_{\text{rf}}) = \frac{1}{2} \frac{1}{V} \sum_{\mathbf{k}} A(\mathbf{k}, \xi_{\mathbf{k}} - \nu_{\text{rf}}) [N_{\text{B}}(\xi_{\mathbf{k}} - \nu_{\text{rf}}) - N_{\text{B}}(\xi_{\mathbf{k},3})], \quad (39)$$

where $\xi_{\mathbf{k},3} = k^2/2 - \mu_3$. In numerical calculation, we take the zero-density or vacuum limit where $\mu_3 < 0$ and $|\mu_3| \gg T$, such that the σ_3 state is nearly empty i.e. $N_{\text{B}}(\xi_{\mathbf{k},3}) = 0$. Now the RF spectrum can be simplified as

$$I(\nu_{\text{rf}}) = \frac{1}{2} \frac{1}{V} \sum_{\bar{\mathbf{k}}} A(\mathbf{k}, \xi_{\mathbf{k}} - \nu_{\text{rf}}) N_{\text{B}}(\xi_{\mathbf{k}} - \nu_{\text{rf}}). \quad (40)$$

Following the analysis in Sec. IV, the RF spectra in our system also contain two features: (i) a single particle peak $I_0(\nu_{\text{rf}})$ inherited from A_0 , corresponding to transferring a free atom from σ_2 to σ_3 , and (ii) the part $I_{\text{int}}(\nu_{\text{rf}})$ corresponding to transferring an atom in bound state or quasi-bound state from σ_2 to σ_3 .

On the BEC side, as shown in Fig. 7(a), $I_0(\nu_{\text{rf}})$ is a delta peak located at $\nu_{\text{rf}} = 0$,

$$I_0(\nu_{\text{rf}}) = \pi \delta(\nu_{\text{rf}}) \frac{1}{V} \sum_{\mathbf{k}} N_{\text{B}}(\xi_{\mathbf{k}}), \quad (41)$$

which is well separated from $I_{\text{int}}(\nu_{\text{rf}})$. $I_{\text{int}}(\nu_{\text{rf}})$ has a threshold at $\nu_{\text{rf}} = -E_b$, since the RF pulse must have

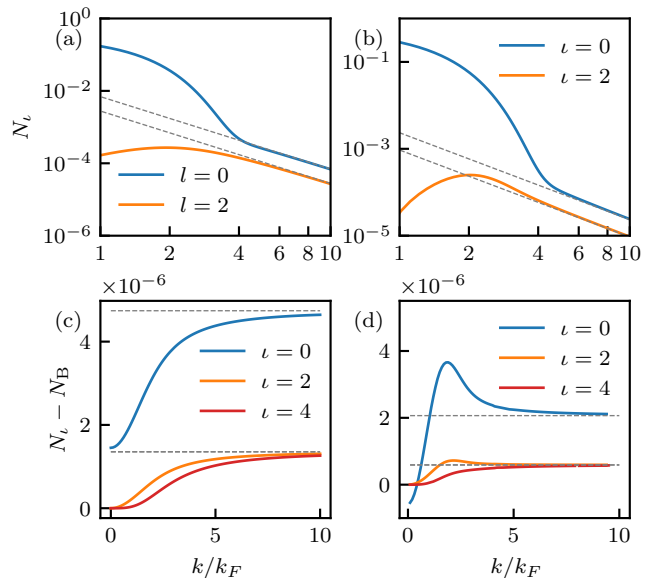


FIG. 6. The momentum distribution projection to Legendre functions. (a) and (b) for p -wave. (c) and (d) for d -wave. The analytic tail in Eq. (35) and Eq. (36) are indicated by gray dashed lines. (a) and (c) are with binding energy $E_b = -2E_F$, while (b) and (d) are with binding energy $E_b = 2E_F$. The results are calculated at temperature $T = 2E_F$. Effective range is $k_F R_p = k_F v_d^{1/3} = 1/30$.

enough energy to break the bound state in order to transfer an atom from σ_2 to σ_3 state.

On the BCS side, the weakly bounded pair has a positive binding energy. Therefore a red detuned RF pulse is enough to transfer the atoms in the weakly bounded pairs to the state σ_3 . The free atom delta peak is expanded and merged into the weakly bounded pairs, as shown in Fig. 7(b)

In the large frequency limit $\nu_{\text{rf}} \rightarrow \infty$, we find the following asymptotic behavior from Eq. (40)

$$I^p(\nu_{\text{rf}}) = \frac{1}{\sqrt{\nu_{\text{rf}}}} C_p, \quad (42)$$

$$I^d(\nu_{\text{rf}}) = \sqrt{\nu_{\text{rf}}} C_d. \quad (43)$$

This also confirms the universal large frequency tail proposed in [23, 24]. The grey dashed line in Fig. 7(b) indicated the contact density in Eq. (26) and Eq. (28) which agrees well with the numerical calculation of Eq. (40).

Next, we investigated the RF spectra at different temperatures, as shown in Fig. 8. On the BEC side, the rf spectrum is more significant at lower temperatures, provided the system is in the normal phase. When the temperature increases, the number of dimers becomes smaller. Therefore the atom number transfer to state σ_3 from a dimer, i.e., the RF spectrum, becomes smaller. However, on the BCS side, because of a positive binding energy, the system tends to form more weakly bounded dimers when the temperature increases. Therefore the

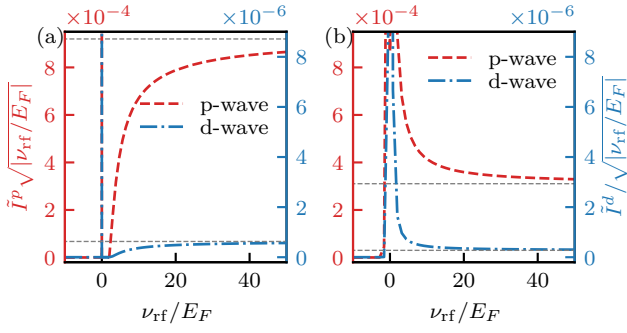


FIG. 7. Dimensionless RF spectra of p -wave and d -wave at temperature $T = 2E_F$. (a) is with binding energy $E_b = -2E_F$. (b) is with binding energy $E_b = 2E_F$. The effective range $k_F R_p = k_F v_d^{1/3} = 1/30$. Grey dashed lines show the tail in Eq. (42) and Eq. (43)

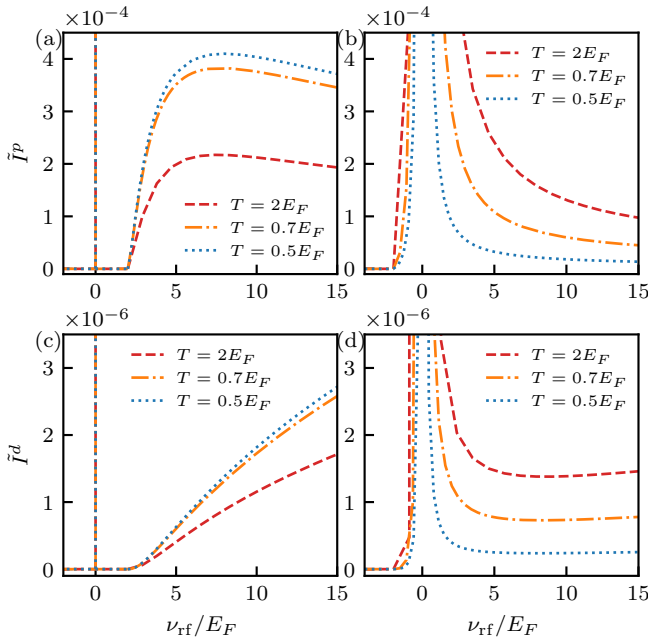


FIG. 8. Dimensionless RF \tilde{I} spectrum at different temperatures. (a) and (b) are for p -wave. (c) and (d) for d -wave. (a) and (c) are with binding energy $E_b = -2E_F$, while (b) and (d) are with binding energy $E_b = 2E_F$. Effective range is $k_F R_p = k_F v_d^{1/3} = 1/30$.

temperature dependence of the RF spectrum on the BCS side shows an opposite behavior. It is worth noting that this reversed temperature dependence was also found in the temperature dependence of the contact density in Fig. 3.

Finally, we give an experiment estimation. In experiments, the number of atoms transferred to the hyperfine state σ_3 in time t obeys the sum rule [4],

$$\int \frac{N_3(\nu_{\text{rf}})}{t} d\nu_{\text{rf}} = \frac{\Omega^2}{2} \pi N, \quad (44)$$

where Ω is the Rabi frequency of RF pulse. The sum rule

of RF spectra in our work is

$$\int \tilde{I}(\tilde{\nu}_{\text{rf}}) d\tilde{\nu}_{\text{rf}} = \frac{1}{2}, \quad (45)$$

where $\tilde{\nu}_{\text{rf}} = \hbar \nu_{\text{rf}} / E_F$, and

$$\tilde{I} = \frac{E_F}{\hbar} \frac{I(\nu_{\text{rf}}) V}{2\pi N}, \quad (46)$$

is the dimensionless RF spectrum.

By comparing Eq. (44) and Eq. (45), we can express the atom number transferred to the hyperfine states σ_3 in time t as

$$N_3 = \frac{\hbar}{E_F} \tilde{I} \cdot \Omega^2 \pi N. \quad (47)$$

For a 10^5 ^{41}K atoms cloud with density 10^{13}cm^{-3} , the estimated $E_F^p = 2^{-2/3} E_F^d \approx 5475\text{Hz}$ where h is Planck constant. For a 0.16ms duration of RF pulse with Rabi frequency $\Omega = 30 \times 2\pi\text{kHz}$, the p -wave RF peak $\tilde{I} \approx 3 \times 10^{-4}$ results in $N_3 \approx 1.6 \times 10^4$, which is about 16% of total atoms, transferred to σ_3 state. For the d -wave RF peak, we find $\tilde{I} \approx 3 \times 10^{-6}$, and transferred atom number is $N_3 \approx 98$, which is about 0.1% of total atom number. It seems that the p -wave RF spectrum might be reachable for the present experiment techniques, while the observation of d -wave signal may be quite a challenge.

VII. SUMMARY

In summary, we studied the p -wave and d -wave interacting Bose quantum gases in the normal phase using Green's function method in the spirit of ladder diagram approximation. Firstly, we derived the contact density, which agrees well with the results of virial expansion. Then, we calculated the single particle spectral function at different directions as well as the momentum distribution. The well known large k tails for p - and d -wave interaction are confirmed. Finally, we obtain the RF spectrum and investigated the temperature dependence of the RF spectrum and discovered a reversed temperature dependence on the BCS and BEC side of FR. We also estimate the transferring rate of atom number under a typical experimental setup. The result for p -wave might be reachable, while for d -wave is quite a challenge.

ACKNOWLEDGMENTS

This work was supported by the National Key Research and Development Program of China (Grant No. 2022YFA1405301 and No. 2018YFA0306502), the National Natural Science Foundation of China (Grant No. 12022405 and No. 11774426), the Beijing Natural Science Foundation (Grant No. Z180013).

-
- [1] I. Bloch, J. Dalibard, and W. Zwerger, *Rev. Mod. Phys.* **80**, 885 (2008).
- [2] S. Giorgini, L. P. Pitaevskii, and S. Stringari, *Rev. Mod. Phys.* **80**, 1215 (2008).
- [3] C. Chin, R. Grimm, P. Julienne, and E. Tiesinga, *Rev. Mod. Phys.* **82**, 1225 (2010).
- [4] C. Luciuk, S. Trotzky, S. Smale, Z. Yu, S. Zhang, and J. H. Thywissen, *Nature Phys* **12**, 599 (2016).
- [5] X.-P. Liu, X.-C. Yao, R. Qi, X.-Q. Wang, Y.-X. Wang, Y.-A. Chen, and J.-W. Pan, *Phys. Rev. A* **98**, 022704 (2018).
- [6] M. Waseem, J. Yoshida, T. Saito, and T. Mukaiyama, *Phys. Rev. A* **98**, 020702 (2018).
- [7] M. Gerken, B. Tran, S. Häfner, E. Tiemann, B. Zhu, and M. Weidemüller, *Phys. Rev. A* **100**, 050701 (2019).
- [8] Y.-T. Chang, R. Senaratne, D. Cavazos-Cavazos, and R. G. Hulet, *Phys. Rev. Lett.* **125**, 263402 (2020).
- [9] D. J. M. Ahmed-Braun, K. G. Jackson, S. Smale, C. J. Dale, B. A. Olsen, S. J. J. M. F. Kokkelmans, P. S. Julienne, and J. H. Thywissen, *Phys. Rev. Res* **3**, 033269 (2021).
- [10] G. Bian, L. Huang, D. Li, Z. Meng, L. Chen, P. Wang, and J. Zhang, *Phys. Rev. A* **106**, 023322 (2022).
- [11] M. Duda, X.-Y. Chen, R. Bause, A. Schindewolf, I. Bloch, and X.-Y. Luo, *Phys. Rev. A* **107**, 053322 (2023).
- [12] V. Venu, P. Xu, M. Mamaev, F. Corapi, T. Bilitewski, J. P. D’Incao, C. J. Fujiwara, A. M. Rey, and J. H. Thywissen, *Nature* **613**, 262 (2023).
- [13] Z. Shi, Z. Li, P. Wang, W. Han, L. Huang, Z. Meng, L. Chen, and J. Zhang, *New J. Phys.* **25**, 023032 (2023).
- [14] Y. Cui, C. Shen, M. Deng, S. Dong, C. Chen, R. Lü, B. Gao, M. K. Tey, and L. You, *Phys. Rev. Lett.* **119**, 203402 (2017).
- [15] X.-C. Yao, R. Qi, X.-P. Liu, X.-Q. Wang, Y.-X. Wang, Y.-P. Wu, H.-Z. Chen, P. Zhang, H. Zhai, Y.-A. Chen, and J.-W. Pan, *Nat. Phys.* **15**, 570 (2019).
- [16] Z. Zhang, L. Chen, K.-X. Yao, and C. Chin, *Nature* **592**, 708 (2021).
- [17] P. Törmä, *Phys. Scr.* **91**, 043006 (2016).
- [18] B. Mukherjee, P. B. Patel, Z. Yan, R. J. Fletcher, J. Struck, and M. W. Zwierlein, *Phys. Rev. Lett.* **122**, 203402 (2019).
- [19] W. E. Liu, Z.-Y. Shi, J. Levinsen, and M. M. Parish, *Phys. Rev. Lett.* **125**, 065301 (2020).
- [20] W. E. Liu, Z.-Y. Shi, M. M. Parish, and J. Levinsen, *Phys. Rev. A* **102**, 023304 (2020).
- [21] P. Nozières and S. Schmitt-Rink, *J Low Temp Phys* **59**, 195 (1985).
- [22] J. Yao, R. Qi, and P. Zhang, *Physical Review A* **97**, 043626 (2018).
- [23] Z. Yu, J. H. Thywissen, and S. Zhang, *Phys. Rev. Lett.* **115**, 135304 (2015).
- [24] P. Zhang, S. Zhang, and Z. Yu, *Phys. Rev. A* **95**, 043609 (2017).
- [25] J. Yao and S. Zhang, *Phys. Rev. A* **97**, 043612 (2018).
- [26] G. C. Strinati, P. Pieri, G. Röpke, P. Schuck, and M. Urban, *Physics Reports* **738**, 1 (2018).
- [27] S. Tan, *Annals of Physics* **323**, 2971 (2008).
- [28] S. Tan, *Annals of Physics* **323**, 2987 (2008).
- [29] S. Tan, *Annals of Physics* **323**, 2952 (2008).
- [30] K. Huang, *Statistical Mechanics. 2nd ed.* (New York: Wiley, 1987).
- [31] X.-J. Liu, *Physics Reports* **524**, 37 (2013).
- [32] E. Beth and G. E. Uhlenbeck, *Physica* **4**, 915 (1937).
- [33] G. D. Mahan, *Many Particle Physics, Third Edition* (Plenum, New York, 2000).